

Finite-momentum mixed singlet-triplet pairing in chiral antiferromagnets induced by even-parity spin texture

Song-Bo Zhang^{1, 2, *} and Lun-Hui Hu^{3, 4, †}

¹*Hefei National Laboratory, Hefei, Anhui, 230088, China*

²*International Center for Quantum Design of Functional Materials (ICQD), University of Science and Technology of China, Hefei, Anhui 230026, China*

³*Center for Correlated Matter and School of Physics, Zhejiang University, Hangzhou 310058, China*

⁴*Department of Applied Physics, Aalto University School of Science, FI-00076 Aalto, Finland*

Non-relativistic spin-splitting in unconventional antiferromagnets has garnered much attention for its promising spintronic applications and open fundamental questions. Here, we uncover a unique even-parity spin texture in chiral non-collinear antiferromagnets, exemplified using a kagome lattice. We consider two distinct types of electrons in the system: one with Schrödinger-like dispersion and the other exhibiting Dirac-like behavior. Remarkably, we show that, for both electron types, this spin texture induces an exotic coexistence of opposite-spin singlet and equal-spin triplet Cooper pairs with finite momentum when proximity-coupled to conventional superconductors. The triplet pairing arises from the intrinsic spin rotation of the antiferromagnet and does not require net magnetization or spin-orbit coupling. Moreover, we identify an unprecedented and tunable phase difference between singlet and triplet pairings, controllable through junction orientation. This mixed pairing state can be experimentally probed via damped oscillations in order parameters and $0\text{-}\pi$ transitions in Josephson junctions. Additionally, we analyze the effect of out-of-plane spin canting, elucidating its role in generating spin-polarized supercurrents, and discuss Mn_3Ga and Mn_3Ge to test our predictions.

Introduction.—Non-relativistic spin splitting, independent of spin-orbit coupling (SOC), can arise in unconventional antiferromagnets or from Fermi-surface instabilities in strongly correlated systems [1–4]. This phenomenon has been observed in antiferromagnets exhibiting large anomalous Hall effect, such as Mn_3Sn [1, 2], and the recently discovered altermagnets [5–13]. Altermagnets belong to a new type of collinear compensated magnetic phase with anisotropic spin splitting. They have been found to exhibit many exotic properties and functionalities [14–17]. In particular, the interplay between altermagnetism and superconductivity has been shown to engender a plethora of unconventional superconducting phenomena [18–31], including finite-momentum Cooper pairing [32, 33] with zero net magnetization [18–20], peculiar Andreev reflections [24–26], and topological superconductivity [27–29]. These intriguing features have garnered growing interest from both theoretical and experimental perspectives [34–50], paving the way for the development of next-generation superconducting devices.

In line with this objective, non-relativistic spin splitting is not the privilege of collinear altermagnets but is also prevalent in non-collinear antiferromagnets [51, 52]. Unlike collinear counterparts, non-collinear antiferromagnets feature diverse spin orientations among adjacent atoms or ions. A notable example is the chiral antiferromagnets (cAFMs), which have been identified in a growing number of materials [1, 2, 53–57], including kagome metals such as Mn_3Sn [2], Mn_3Pt [58], Mn_3Ge [59, 60], Mn_3Ga [61, 62] and Mn_3Ir [63]. Recent experimental efforts have involved Josephson junctions using Mn_3Ge thin films [64, 65]. In contrast to collinear altermagnets, spin is not conserved in cAFMs, leading to non-trivial spin textures that could

preserve parity [51, 52]. Nevertheless, investigations into the fundamental interplay between even-parity spin texture and superconductivity in junctions are surprisingly scarce. This gap offers an opportunity to explore new mechanisms for generating spin-triplet pairing, beyond known scenarios, such as (i) magnetic noncollinearity at ferromagnet/superconductor interfaces [66–72]; (ii) odd-parity spin textures induced by SOC [73–82]; and (iii) collinear Néel antiferromagnet/superconductor junctions with spin-active interfaces or spin canting [83–88].

In this work, we study a unique even-parity spin texture in cAFMs and explore its role in proximity-induced pairing correlations in cAFM coupled to conventional s -wave superconductors. We discover a mixed singlet-triplet pairing state, wherein both components exhibit finite center-of-mass momentum, akin to the Fulde-Ferrell-Larkin-Ovchinnikov (FFLO) state, but with a trade-off behavior between them. While the singlet pairing exhibits even parity in both frequency and antiferromagnetic order, the triplet pairings are odd in these aspects. Moreover, the relative phase between the singlet and triplet amplitudes can be controlled by adjusting the junction orientation. We illustrate this SOC-free mechanism for generating triplet pairing through general symmetry analysis and, as a concrete example, by examining the cAFM on a kagome lattice. We construct low-energy effective models for the system and analytically show that the finite-momentum Cooper pairs are associated with inter-band pairing. For experimental implications for candidate materials such as Mn_3Ge and Mn_3Ga , we find that out-of-plane spin canting causes one of the equal-spin triplet amplitudes to predominate, thus facilitating spin-polarized supercurrents.

Mixed singlet-triplet pairing from even-parity spin texture.— Non-relativistic spin-split bands can be classified by spin-space group, which involves rotation operators acting independently on space and spin coordinates [11, 12, 55–57, 89, 90]. For concreteness, we consider the non-collinear cAFM phase on the kagome lattice [Fig. 1(a)]. This phase can be characterized by $\{U_z(\frac{2\pi}{3})||C_z(\frac{\pi}{3})\}$, which combines a six-fold spatial rotation $C_z(\frac{\pi}{3})$ and a three-fold spin rotation $U_z(\frac{2\pi}{3})$ about z -axis. Additional symmetries include $\{U_x(\pi)||C_x(\pi)\}$ (reflection), $\{E||\mathcal{I}\}$ (inversion) and $\{U_z(\pi)\mathcal{T}||\mathcal{I}\}$ (mirror), where \mathcal{I} and \mathcal{T} are inversion and time-reversal symmetries, respectively. These operators g expand the little group at the Γ point in momentum space, determining the spin texture of each band by satisfying $g\mathbf{S}(\mathbf{k})g^{-1} = \mathbf{S}(g\mathbf{k})$, where $\mathbf{S}(\mathbf{k})$ denotes the spin polarization of a state with momentum $\mathbf{k} = (k_x, k_y)$. The in-plane reflection enforces $S_z(\mathbf{k}) = 0$, while both in-plane components are even in \mathbf{k} due to inversion symmetry, as denoted by $\mathbf{S}(\mathbf{k}) = \mathbf{S}(-\mathbf{k})$. Thus, we refer to this as the even-parity spin texture. More details can be found in the Supplemental Material (SM) [91]. It fundamentally differs from the odd-parity spin texture arising from SOC, which obeys $\mathbf{S}(\mathbf{k}) = -\mathbf{S}(-\mathbf{k})$.

The even-parity spin texture drives the emergence of mixed singlet-triplet pairing in the cAFM in proximity to a conventional superconductor. To elucidate the basic mechanism, we present an intuitive picture in Fig. 1(b). Given proximity-induced singlet Cooper pairs, only interband pairing is allowed due to the even-parity spin texture [91]. For illustration, we consider a junction oriented along x -direction, with dominant electronic states spin-polarized in x -direction. In this case, electrons with spin \uparrow_{1x} at $-\bar{k}_+$ (\downarrow_{1x} at $-\bar{k}_-$) must pair with those with \downarrow_{2x} at \bar{k}_- (\uparrow_{2x} at \bar{k}_+). The pairing may occur non-locally in time, as the subscripts 1 and 2 imply. Thus, the Cooper pairs carry finite center-of-mass momentum given by $\pm Q = \pm(\bar{k}_- - \bar{k}_+)$. The pairing amplitude acquires spatially varying phases $e^{\pm iQx}$, resulting in an FFLO-like state [72], i.e., $\uparrow_{1x}\downarrow_{2x} e^{iQx} - \downarrow_{1x}\uparrow_{2x} e^{-iQx}$. To reveal equal-spin triplet component polarized in z -direction, a spin rotation can be performed as $\uparrow_{\nu z} = (\uparrow_{\nu x} + \downarrow_{\nu x})/\sqrt{2}$ and $\downarrow_{\nu z} = (\uparrow_{\nu x} - \downarrow_{\nu x})/\sqrt{2}$ with $\nu \in \{1, 2\}$ that are eigenstates of s_z . This yields a mixed singlet-triplet pairing $(\downarrow_{1z}\uparrow_{2z} - \uparrow_{1z}\downarrow_{2z})\cos(Qx) + i(\uparrow_{1z}\uparrow_{2z} - \downarrow_{1z}\downarrow_{2z})\sin(Qx)$. According to the Pauli principle, these s -wave triplet components are only permitted for the non-static case, implying that they are odd in frequency [68, 92, 93].

Moreover, this argument holds for junctions oriented in any other direction, where dominant electronic states are spin-polarized in different directions. The mixed pairing reads generally $(\downarrow_{1z}\uparrow_{2z} - \uparrow_{1z}\downarrow_{2z})\cos(Qx) + i(e^{i2\phi}\uparrow_{1z}\uparrow_{2z} - e^{-i2\phi}\downarrow_{1z}\downarrow_{2z})\sin(Qx)$, where ϕ is the junction orientation relative to x -axis and factor 2 reflects the symmetry $\{U_z(\frac{2\pi}{3})||C_z(\frac{\pi}{3})\}$. Thus, when ϕ varies, the phases of the triplet components change, while the phase of the singlet component remains the same as that in the superconduc-

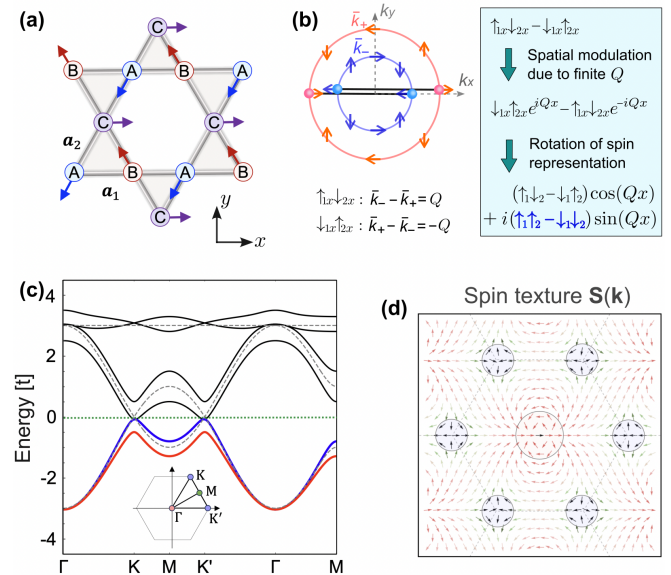


Fig. 1. (a) Crystal structure of the kagome antiferromagnet with a 120° cAFM order. The arrows on the three sublattices A, B, C indicate the local magnetic moments. \mathbf{a}_1 and \mathbf{a}_2 are nearest-neighbor vectors. (b) Creation mechanism of mixed singlet and equal-spin triplet pairing. For illustration, we consider the spins along x -direction and thus have two Cooper pairs with opposite center-of-mass momenta $\pm Q$. (c) Band structure along high symmetry lines in the absence (dashed) and presence (solid) of cAFM order. The inset shows the first Brillouin zone with the high symmetry points indicated. (d) Even-parity spin texture of the lowest band in the Brillouin zone. Parameters are $t = 1$ and $J = 0.3t$.

tor. This analysis shows that opposite-spin triplet pairing correlation vanishes, aligning with the symmetry analysis provided in the SM [91] and validated by our numerical calculations [Fig. 3(c)]

Hence, the even-parity spin texture uniquely induces the mixed singlet-triplet pairing at finite frequencies in the junction. It showcases several intriguing features: (i) equal magnitudes for two equal-spin triplet components, (ii) a trade-off in the spatial oscillations between singlet and triplet components, (iii) a tunable π -periodic phase difference between singlet and triplet components controlled by junction orientation, and (iv) no need for net magnetization, SOC, multi-band superconductivity, spin-active interfaces, or large-scale magnetic inhomogeneities (e.g., domain walls). Below, we verify these features numerically and analytically, establishing this mixed pairing as a novel state distinct from previous proposals [66–88, 92–96].

Odd-frequency equal-spin triplet pairing.— To validate the general analysis above, we consider a tight-binding model on the kagome lattice [1, 89],

$$\mathcal{H}(\mathbf{k}) = \begin{pmatrix} t & f_{1,\mathbf{k}} & f_{2,\mathbf{k}} \\ f_{1,\mathbf{k}} & t & f_{3,\mathbf{k}} \\ f_{2,\mathbf{k}} & f_{3,\mathbf{k}} & t \end{pmatrix} s_0 + \begin{pmatrix} \mathbf{d}_A & 0 & 0 \\ 0 & \mathbf{d}_B & 0 \\ 0 & 0 & \mathbf{d}_C \end{pmatrix} \cdot \mathbf{s}, \quad (1)$$

where $f_{i,\mathbf{k}} = -2t \cos(\mathbf{k} \cdot \mathbf{a}_i)$, t is the strength of nearest-neighbor hopping between s -electrons and is taken as energy unit. The three nearest-neighbor vectors are defined as $\mathbf{a}_1 = (1, 0)$, $\mathbf{a}_2 = (1, \sqrt{3})/2$, and $\mathbf{a}_3 = \mathbf{a}_2 - \mathbf{a}_1$. For concreteness, we consider a 120° cAFM configuration with local magnetic moments $\mathbf{d}_j = J(\cos \theta_j, \sin \theta_j, 0)$, where J measures the strength and $\theta_{A/B/C} = \{4\pi/3, 2\pi/3, 0\}$. The band structure for $J = 0$ along high-symmetry lines is depicted in Fig. 1(c) [dashed curves]. It possesses Schrödinger-like and Dirac-like electrons at the band edge (around the Γ point) or center (around the K/K' point), respectively. The presence of $J \neq 0$ breaks the spin degeneracy of the band structure [solid lines in Fig. 1(c)], and leads to even-parity spin textures for both types of electrons [Fig. 1(d)].

We compute the pairing correlations in an s -wave superconductor/cAFM junction oriented along x -direction from the anomalous Matsubara Green function, using a recursive technique [97, 98]. The superconducting lead is modeled on the same kagome lattice without magnetism but a uniform s -wave pairing potential, described by $H_\Delta = \sum_{i,\alpha \in \{A,B,C\}} (\Delta c_{i,\alpha,\uparrow}^\dagger c_{i,\alpha,\downarrow}^\dagger + h.c.)$, where i runs over all unit cells and α labels the three sublattices. For simplicity, we impose translation symmetry in y -direction. The anomalous Green function is decomposed into [99]

$$\mathbf{G}_{eh} = -is_y \sum_{j=0,x,y,z} \mathbf{f}_j(x, x', k_y, i\omega) s_j, \quad (2)$$

where \mathbf{f}_0 corresponds to the singlet, and \mathbf{f}_z as well as $\mathbf{f}_{\uparrow\uparrow/\downarrow\downarrow} = \mp \mathbf{f}_x - i\mathbf{f}_y$ are triplet amplitudes. x and x' denote layer positions of unit cells of the kagome lattice along x -axis, and ω the Matsubara frequency. We focus on local pairings with $x = x'$. Summing over the three sublattices within each unit cell, we obtain the pairing amplitudes as $\mathcal{F}_j(x, k_y, \omega) = \text{Tr}[\mathbf{f}_j(x, x, k_y, i\omega)]$, where $j \in \{0, z, \uparrow\uparrow, \downarrow\downarrow\}$. We use the parameters $J = 0.5t$ and $\Delta = 0.1t$ in the calculations.

Figure 2 presents the results for $k_y = 0$ and a chemical potential near the band edge (i.e., $\mu = -2.5t$). We observe a purely real singlet amplitude \mathcal{F}_0 induced in the cAFM, even at finite frequency ω . It maximizes in the static limit ($\omega = 0$) and decays monotonically to zero as $|\omega|$ grows. For $|\omega| < \Delta$, pronounced oscillations around zero appear near the interface, similar to the FFLO state [Fig. 2(a)]. More strikingly, for $\omega \neq 0$, while $\mathcal{F}_z = 0$, two purely imaginary equal-spin triplet components emerge and have the same amplitudes, $\mathcal{F}_{\downarrow\downarrow} = -\mathcal{F}_{\uparrow\uparrow} = i\mathcal{F}_t$ [Fig. 2(b)]. \mathcal{F}_t is odd in ω , in contrast to \mathcal{F}_0 . It is of the same order of magnitude and oscillates in x as \mathcal{F}_0 . In a nonmagnetic metal ($J = 0$), only the singlet pairing exists ($\mathcal{F}_0 \neq 0$ but $\mathcal{F}_z = \mathcal{F}_t = 0$) [Fig. 2(c)]. Once $J \neq 0$ is present, FFLO-like pairings are developed in both singlet and equal-spin triplet channels at finite ω , as evidenced in Fig. 2(d). This comparison demonstrates that the mixed singlet-triplet pairing is driven by the even-parity spin texture stemming from the cAFM order. Additionally, the

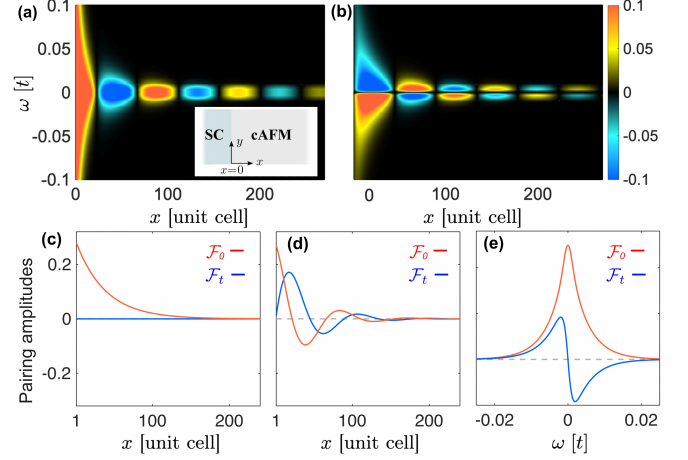


Fig. 2. (a) Singlet amplitude \mathcal{F}_0 (in units of t^{-1}) as a function of frequency ω and position x (in units of unit-cell layers) in the cAFM. Inset sketches the SC-cAFM junction oriented in x -direction. (b) Same as (a) but for equal-spin triplet pairing amplitudes, $\mathcal{F}_t = i\mathcal{F}_{\uparrow\uparrow} = -i\mathcal{F}_{\downarrow\downarrow}$. (c) \mathcal{F}_0 (red) and \mathcal{F}_t (blue) as functions of x in the cAFM for $J = 0$ and $\omega = 0.1\Delta$. (d) Same as (c) but for a finite cAFM order ($J = 0.5t$). (e) \mathcal{F}_0 (red) and \mathcal{F}_t (blue) as functions of ω for $x = 80$.

oscillations of \mathcal{F}_0 and \mathcal{F}_t appear to have a $\pi/2$ difference in phase, resembling a trade-off between them.

Moreover, as ω increases, \mathcal{F}_t undergoes a rapid increase until reaching a maximum value, followed by a monotonic decay to zero [Figs. 2(b) and 2(e)]. The amplitude of \mathcal{F}_t increases as J increases, and flips sign when J flips sign. The results of summing over all k_y are provided in the SM [91], showing qualitatively the same features. We also examine the proximity effect for other energy regimes and demonstrate that these intriguing observations persist [91]. Rotating the junction orientation varies the phases of $\mathcal{F}_{\uparrow\uparrow(\downarrow\downarrow)}$. All these results agree with our general argument.

Finite-momentum Cooper pairing.— Next, we prove the emergence of finite-momentum pairing analytically. Since the singlet and triplet pairings share the same finite momentum at any frequency, it is sufficient to consider only the singlet pairing in the static limit. To this end, we derive two representative low-energy effective Hamiltonians near the band edge ($E_{\text{edge}} = -3t$) and center ($E_{\text{cen}} = 0$), respectively (see SM [91] for derivation). The first one showcases Schrödinger-like electrons around the Γ point,

$$\mathcal{H}_\Gamma(\mathbf{k}) = t(k_x^2 + k_y^2)s_0 + m_\Gamma[(k_x^2 - k_y^2)s_x - 2k_x k_y s_y], \quad (3)$$

where $m_\Gamma = J/12$ [91, 100, 101]. The second model features Dirac-like electrons around the K/K' points,

$$\mathcal{H}_{K(K')}(\mathbf{k}) = \chi v(k_x \sigma_1 + k_y \sigma_3)s_0 + m_K(\sigma_1 s_x - \sigma_3 s_y), \quad (4)$$

with $v = \sqrt{3}t$, $m_K = J/2$, $\chi = +1$ (-1) for the valley around the K (K') point, and σ_i are Pauli matrices acting on pseudospin. Using the approach of Cooper-pair propagator, we calculate observables such as local pairing

correlations and Josephson supercurrent [91]. Explicitly, for large widths and Fermi surfaces, the induced pairing correlations $\langle|\Psi(\mathbf{r})|\rangle$ for the Schrödinger and Dirac electrons can be found as

$$\langle|\Psi(\mathbf{r})|\rangle_{\Gamma(K)} \propto \frac{1}{x^{3/2}} \cos \left(Q_{\Gamma(K)} x - \frac{\pi}{4} \right), \quad (5)$$

where we have $Q_{\Gamma} \approx \sqrt{\mu_{\Gamma} m_{\Gamma}}$ and $Q_K \approx 2m_K/v$ for small J . The spatial oscillation of $\langle|\Psi(\mathbf{r})|\rangle_{\Gamma(K)}$ agrees well with our numerical findings. The periodicity of both oscillations is determined by the Cooper-pair momentum, i.e., $P_{\Gamma(K)} = 2\pi/Q_{\Gamma/K}$. Interestingly, P_{Γ} increases as μ_{Γ} decreases, while P_K remains independent of μ_K , which may be experimentally verified. In the SM [91], we further calculate supercurrents in Josephson junctions and show that the finite-momentum pairing generates $0-\pi$ transitions, which can be achieved by adjusting junction length or gating/doping on the cAFM.

Spin canting and experimental implications.— As discussed above, the equal-spin triplet pairings $\mathcal{F}_{\uparrow\uparrow/\downarrow\downarrow}$ exhibit equal magnitude. However, real materials may have out-of-plane spin canting, as signified by sizable anomalous Hall effects in experiments [59]. This spin canting induces a weak net magnetization and makes one triplet component predominant. To illustrate this, we capture the spin canting M_z by incorporating an additional Zeeman term into the model. Thus, the inclusion of $M_z s_z$ (or $M_z s_z \sigma_0$) in the effective Hamiltonians in Eqs. (3) and (4) gives rise to the band splitting and the opening of spin gaps at both Γ and K/K' points [Fig. 3(a)].

In Fig. 3, we calculate numerically the pairing correlations with the kagome lattice model to explore the effect of M_z . We find that the triplet amplitudes $\mathcal{F}_{\uparrow\uparrow/\downarrow\downarrow}$ remain purely imaginary, while the singlet one \mathcal{F}_0 is real-valued. Their trade-off behavior persists [Fig. 3(b)]. A finite opposite-spin triplet component \mathcal{F}_z (corresponding to $\uparrow\downarrow + \downarrow\uparrow$) emerges as well, which is purely imaginary and oscillates in phase with $\mathcal{F}_{\uparrow\uparrow/\downarrow\downarrow}$. Interestingly, a finite M_z indeed creates an imbalance between $\mathcal{F}_{\uparrow\uparrow}$ and $\mathcal{F}_{\downarrow\downarrow}$. Both $\mathcal{F}_{\uparrow\uparrow/\downarrow\downarrow}$ are generally suppressed by increasing M_z . However, they are suppressed differently, resulting in a substantial discrepancy between them. For positive M_z , we have always $|\mathcal{F}_{\uparrow\uparrow}| > |\mathcal{F}_{\downarrow\downarrow}|$, while for negative M_z , $|\mathcal{F}_{\uparrow\uparrow}| < |\mathcal{F}_{\downarrow\downarrow}|$ (detailed in the SM [91]).

In Fig. 3(c), we calculate the maximum values of $|\mathcal{F}_{\uparrow\uparrow/\downarrow\downarrow}|$ and their difference as a function of M_z . For a small canting tendency, $\mathcal{F}_{\uparrow\uparrow}$ and $\mathcal{F}_{\downarrow\downarrow}$ decrease monotonically at rather different rates as M_z increases. Figure 3(d) shows the ratio $\max(|\mathcal{F}_{\uparrow\uparrow}|)/\max(|\mathcal{F}_{\downarrow\downarrow}|)$ as a function of M_z [102]. This ratio increases monotonically as M_z grows for any frequencies. Thus, a stronger M_z yields more excess Cooper pairs with specific spin polarization, implying a net spin supercurrent in the superconducting junctions. These general features occur for both Schrödinger and Dirac electrons. Note that instead of spin-canting, a significant M_z could also originate from orbital magnetization

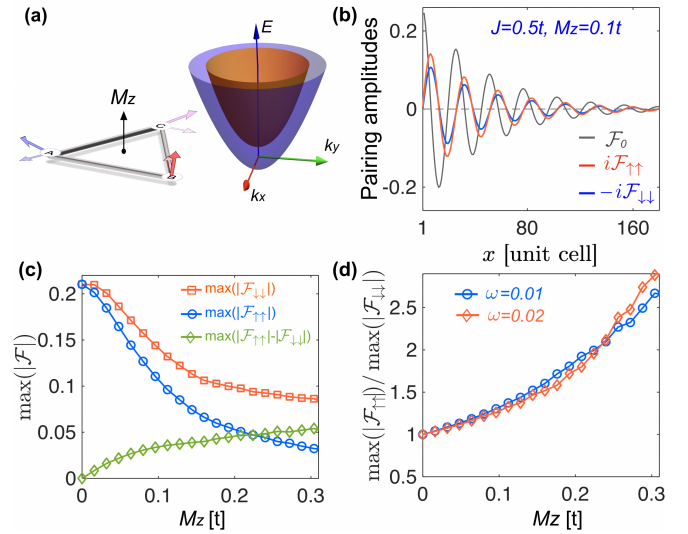


Fig. 3. (a) Schematic of out-of-plane canting on the cAFM and the band structure near the band edge. (b) Spin-singlet (black) and equal-spin-triplet amplitudes (red and blue), \mathcal{F}_0 , $\mathcal{F}_{\uparrow\uparrow}$ and $\mathcal{F}_{\downarrow\downarrow}$ (in units of t^{-1}), as functions of position x in the cAFM under out-of-plane spin canting (i.e., $J = 0.5t$ and $M_z = 0.1t$). (c) $\max(|\mathcal{F}_{\uparrow\uparrow}|)$, $\max(|\mathcal{F}_{\downarrow\downarrow}|)$ and their difference as functions of canting strength M_z . (d) $\max(|\mathcal{F}_{\uparrow\uparrow}|)/\max(|\mathcal{F}_{\downarrow\downarrow}|)$ as a function of M_z . Other parameters: $\mu = \mu_s = -2t$, $\omega = 0.01t$ and $\Delta = 0.05t$.

under an external magnetic field [103], leading to the same conclusion.

Finally, we discuss cAFM candidate materials Mn_3Ga and Mn_3Ge [59–62] as possible platforms for testing our predictions. The band structures of these materials have been investigated using *ab initio* calculations [104], showing pronounced spin-split electronic states with quadratic dispersion around the Γ point. We estimate the shifts in μ needed to bring the quadratic electrons to the Fermi level, which are around -0.1 eV and -0.3 eV for Mn_3Ga and Mn_3Ge , respectively [105]. For Mn_3Ga with Néel temperature 470 K, a significant spin splitting $m_{\Gamma}/t = 0.35$ can be estimated for the effective model in Eq. (3). Using $\mu_{\Gamma} \equiv \mu - E_{\text{edge}} = 0.1\text{--}0.3t$ in Eq. (3) and the lattice constant of $a = 0.53$ nm, we estimate the oscillation periodicity of order parameters and Josephson currents as $\sim 2\pi a t / (\sqrt{\mu_{\Gamma}/t} m_{\Gamma}) \approx 17\text{--}30$ nm. This suggests that $0\text{--}\pi$ transitions could be observed in Josephson junctions with lengths exceeding 30 nm, a feasible length scale within current experimental settings. For Mn_3Ge , the Néel temperature is around 380 K and the cAFM phase remains robust at low temperatures [64, 65]. The spin splitting is weaker ($m_{\Gamma}/t \sim 0.1$), compared to Mn_3Ga . Thus, for the same μ_{Γ} , the oscillation periodicity would be larger.

Conclusions and discussions.— In summary, we have proposed a general theory for creating mixed singlet-triplet pairing states through even-parity spin texture in cAFMs that preserve inversion symmetry. For kagome systems,

our general symmetry analysis, numerical calculations, and analytical results have consistently demonstrated that the even-parity spin texture gives rise to a mixed state of even-frequency singlet and odd-frequency equal-spin triplet Cooper pairs with finite momentum in the cAFM when interfaced with conventional superconductors. These finite-momentum pairings can be detected via damped oscillations in order parameters and controllable $0\text{-}\pi$ transitions in Josephson junctions. Additionally, we have shown that the out-of-plane spin canting leads to an imbalance between Cooper pairs with opposite spins. This work demonstrates the singlet-triplet mixed state is not a privilege of spin-orbit coupled system but more broadly associated with the spin texture. In realistic systems, inhomogeneity might exist in the interfaces, leading to spatial variations in the coupling between the cAFM and the superconductor. However, as long as these variations are much smaller than the average coupling strength, our results remain qualitatively unaffected.

While our discussion primarily focuses on kagome-type systems, our main findings also apply to other lattice structures hosting the cAFM phase [106], such as in the Mn_3AN family ($A = \text{Ni}, \text{Ga}, \text{Sn}$) with triangular lattices and new candidate materials enumerated in recent studies [55–57].

We thank Qian Niu and Zhenyu Zhang for valuable discussions. S.B.Z. was supported by the start-up fund at HFNL, the Innovation Program for Quantum Science and Technology (Grant No. 2021ZD0302801), and Anhui Initiative in Quantum Information Technologies (Grant No. AHY170000). L.H.H. at Aalto is funded by the Jane and Aatos Erkko Foundation and the Keele Foundation as part of the SuperC collaboration.

-
- * songbozhang@ustc.edu.cn; equally contribution
† lunhui@zju.edu.cn; equally contribution
- [1] H. Chen, Q. Niu, and A. H. MacDonald, *Phys. Rev. Lett.* **112**, 017205 (2014).
 - [2] S. Nakatsuji, N. Kiyohara, and T. Higo, *Nature* **527**, 212 (2015).
 - [3] C. Wu and S.-C. Zhang, *Phys. Rev. Lett.* **93**, 036403 (2004).
 - [4] C. Wu, K. Sun, E. Fradkin, and S.-C. Zhang, *Phys. Rev. B* **75**, 115103 (2007).
 - [5] L. Šmejkal, R. González-Hernández, T. Jungwirth, and J. Sinova, *Sci. Adv.* **6**, eaaz8809 (2020).
 - [6] M. Naka, S. Hayami, H. Kusunose, Y. Yanagi, Y. Motome, and H. Seo, *Nat. Commun.* **10**, 4305 (2019).
 - [7] S. Hayami, Y. Yanagi, and H. Kusunose, *J. Phys. Soc. Jpn.* **88**, 123702 (2019).
 - [8] L.-D. Yuan, Z. Wang, J.-W. Luo, E. I. Rashba, and A. Zunger, *Phys. Rev. B* **102**, 014422 (2020).
 - [9] I. I. Mazin, K. Koepernik, M. D. Johannes, R. González-Hernández, and L. Šmejkal, *Proc. Nat. Acad. Sci.* **118**, e2108924118 (2021).
 - [10] H.-Y. Ma, M. Hu, N. Li, J. Liu, W. Yao, J.-F. Jia, and J. Liu, *Nat. Commun.* **12**, 2846 (2021).
 - [11] L. Šmejkal, J. Sinova, and T. Jungwirth, *Phys. Rev. X* **12**, 031042 (2022).
 - [12] L. Šmejkal, J. Sinova, and T. Jungwirth, *Phys. Rev. X* **12**, 040501 (2022).
 - [13] K.-H. Ahn, A. Hariki, K.-W. Lee, and J. Kuneš, *Phys. Rev. B* **99**, 184432 (2019).
 - [14] D.-F. Shao, S.-H. Zhang, M. Li, C.-B. Eom, and E. Y. Tsymbal, *Nat. Commun.* **12**, 7061 (2021).
 - [15] Z. Feng, X. Zhou, L. Šmejkal, L. Wu, Z. Zhu, H. Guo, R. González-Hernández, X. Wang, H. Yan, P. Qin, *et al.*, *Nat. Electron.* **5**, 735 (2022).
 - [16] L. Šmejkal, A. B. Hellenes, R. González-Hernández, J. Sinova, and T. Jungwirth, *Phys. Rev. X* **12**, 011028 (2022).
 - [17] H.-J. Lin, S.-B. Zhang, H.-Z. Lu, and X. C. Xie, *Phys. Rev. Lett.* **134**, 136301 (2025).
 - [18] S.-B. Zhang, L.-H. Hu, and T. Neupert, *Nat. Commun.* **15**, 1801 (2024).
 - [19] S. Sumita, M. Naka, and H. Seo, *Phys. Rev. Res.* **5**, 043171 (2023).
 - [20] D. Chakraborty and A. M. Black-Schaffer, *Phys. Rev. B* **110**, L060508 (2024).
 - [21] J. A. Ouassou, A. Brataas, and J. Linder, *Phys. Rev. Lett.* **131**, 076003 (2023).
 - [22] C. W. J. Beenakker and T. Vakhtel, *Phys. Rev. B* **108**, 075425 (2023).
 - [23] Q. Cheng and Q. Sun, *Phys. Rev. B* **109**, 024517 (2024).
 - [24] C. Sun, A. Brataas, and J. Linder, *Phys. Rev. B* **108**, 054511 (2023).
 - [25] M. Papaj, *Phys. Rev. B* **108**, L060508 (2023).
 - [26] M. Wei, L. Xiang, F. Xu, L. Zhang, G. Tang, and J. Wang, *Phys. Rev. B* **109**, L201404 (2024).
 - [27] D. Zhu, Z.-Y. Zhuang, Z. Wu, and Z. Yan, *Phys. Rev. B* **108**, 184505 (2023).
 - [28] Y.-X. Li and C.-C. Liu, *Phys. Rev. B* **108**, 205410 (2023).
 - [29] S. A. A. Ghorashi, T. L. Hughes, and J. Cano, *Phys. Rev. Lett.* **133**, 106601 (2024).
 - [30] S. Banerjee and M. S. Scheurer, *Phys. Rev. B* **110**, 024503 (2024).
 - [31] H.-P. Sun, S.-B. Zhang, C.-A. Li, and B. Trauzettel, *Phys. Rev. B* **111**, 165406 (2025).
 - [32] P. Fulde and R. A. Ferrell, *Phys. Rev.* **135**, A550 (1964).
 - [33] A. I. Larkin and Y. N. Ovchinnikov, *Zh. Eksp. Teor. Fiz.* **47**, 1136 (1964).
 - [34] S. Lee, S. Lee, S. Jung, J. Jung, D. Kim, Y. Lee, B. Seok, J. Kim, B. G. Park, L. Šmejkal, C.-J. Kang, and C. Kim, *Phys. Rev. Lett.* **132**, 036702 (2024).
 - [35] X. Zhou, W. Feng, R.-W. Zhang, L. Šmejkal, J. Sinova, Y. Mokrousov, and Y. Yao, *Phys. Rev. Lett.* **132**, 056701 (2024).
 - [36] O. Fedchenko, J. Minář, A. Akashdeep, S. W. D'Souza, D. Vasilyev, O. Tkach, L. Odenbreit, Q. Nguyen, D. Kutnyakhov, N. Wind, *et al.*, *Sci. Adv.* **10**, eadj4883 (2024).
 - [37] L. Han, X. Fu, R. Peng, X. Cheng, J. Dai, L. Liu, Y. Li, Y. Zhang, W. Zhu, H. Bai, *et al.*, *Sci. Adv.* **10**, eadn0479 (2024).
 - [38] X. Feng, H. Bai, X. Fan, M. Guo, Z. Zhang, G. Chai, T. Wang, D. Xue, C. Song, and X. Fan, *Phys. Rev. Lett.* **132**, 086701 (2024).
 - [39] T. Osumi, S. Souma, T. Aoyama, K. Yamauchi, A. Honma, K. Nakayama, T. Takahashi, K. Ohgushi, and T. Sato, *Phys. Rev. B* **109**, 115102 (2024).
 - [40] H. Chen, L. Liu, X. Zhou, Z. Meng, X. Wang, Z. Duan,

- G. Zhao, H. Yan, P. Qin, and Z. Liu, *Adv. Mater.*, **2310379** (2024).
- [41] S. Bhowal and N. A. Spaldin, *Phys. Rev. X* **14**, 011019 (2024).
- [42] S.-W. Cheong and F.-T. Huang, *npj Quantum Materials* **9**, 13 (2024).
- [43] M. Roig, A. Kreisel, Y. Yu, B. M. Andersen, and D. F. Agterberg, *Phys. Rev. B* **110**, 144412 (2024).
- [44] L.-D. Yuan, A. B. Georgescu, and J. M. Rondinelli, *Phys. Rev. Lett.* **133**, 216701 (2024).
- [45] J.-X. Hu, O. Matsyshyn, and J. C. W. Song, *Phys. Rev. Lett.* **134**, 026001 (2025).
- [46] A. A. Zyuzin, arXiv:2402.15459 (2024).
- [47] R. He, D. Wang, N. Luo, J. Zeng, K.-Q. Chen, and L.-M. Tang, *Phys. Rev. Lett.* **130**, 046401 (2023).
- [48] Y.-P. Zhu, X. Chen, X.-R. Liu, Y. Liu, P. Liu, H. Zha, G. Qu, C. Hong, J. Li, Z. Jiang, *et al.*, *Nature* **626**, 523 (2024).
- [49] J. Krempaský, L. Šmejkal, S. D’Souza, M. Hajlaoui, G. Springholz, K. Uhlířová, F. Alarab, P. Constantinou, V. Strocov, D. Usanov, *et al.*, *Nature* **626**, 517 (2024).
- [50] S. Reimers, L. Odenbreit, L. Šmejkal, V. N. Strocov, P. Constantinou, A. B. Hellenes, R. Jaeschke Ubiergo, W. H. Campos, V. K. Bharadwaj, A. Chakraborty, *et al.*, *Nat. Commun.* **15**, 2116 (2024).
- [51] T. Jungwirth, X. Marti, P. Wadley, and J. Wunderlich, *Nat. Nanotech.* **11**, 231 (2016).
- [52] L. Šmejkal, A. H. MacDonald, J. Sinova, S. Nakatsuji, and T. Jungwirth, *Nat. Rev. Mater.* **7**, 482 (2022).
- [53] V. Baltz, A. Manchon, M. Tsoi, T. Moriyama, T. Ono, and Y. Tserkovnyak, *Rev. Mod. Phys.* **90**, 015005 (2018).
- [54] A. Manchon, J. Železný, I. M. Miron, T. Jungwirth, J. Sinova, A. Thiaville, K. Garello, and P. Gambardella, *Rev. Mod. Phys.* **91**, 035004 (2019).
- [55] Y. Jiang, Z. Song, T. Zhu, Z. Fang, H. Weng, Z.-X. Liu, J. Yang, and C. Fang, *Phys. Rev. X* **14**, 031039 (2024).
- [56] X. Chen, J. Ren, Y. Zhu, Y. Yu, A. Zhang, P. Liu, J. Li, Y. Liu, C. Li, and Q. Liu, *Phys. Rev. X* **14**, 031038 (2024).
- [57] Z. Xiao, J. Zhao, Y. Li, R. Shindou, and Z.-D. Song, *Phys. Rev. X* **14**, 031037 (2024).
- [58] Z. Liu, H. Chen, J. Wang, J. Liu, K. Wang, Z. Feng, H. Yan, X. Wang, C. Jiang, J. Coey, *et al.*, *Nat. Electron.* **1**, 172 (2018).
- [59] N. Kiyohara, T. Tomita, and S. Nakatsuji, *Phys. Rev. Appl.* **5**, 064009 (2016).
- [60] A. K. Nayak, J. E. Fischer, Y. Sun, B. Yan, J. Karel, A. C. Komarek, C. Shekhar, N. Kumar, W. Schnelle, J. Kübler, *et al.*, *Sci. Adv.* **2**, e1501870 (2016).
- [61] Z. Liu, Y. Zhang, G. Liu, B. Ding, E. Liu, H. M. Jafri, Z. Hou, W. Wang, X. Ma, and G. Wu, *Scientific Reports* **7**, 515 (2017).
- [62] L. Song, F. Zhou, H. Li, B. Ding, X. Li, X. Xi, Y. Yao, Y.-C. Lau, and W. Wang, *Adv. Funct. Mater.* **2024**, 2316588 (2024).
- [63] W. Zhang, W. Han, S.-H. Yang, Y. Sun, Y. Zhang, B. Yan, and S. S. Parkin, *Sci. Adv.* **2**, e1600759 (2016).
- [64] K.-R. Jeon, B. K. Hazra, K. Cho, A. Chakraborty, J.-C. Jeon, H. Han, H. L. Meyerheim, T. Kontos, and S. S. Parkin, *Nat. Mater.* **20**, 1358 (2021).
- [65] K.-R. Jeon, B. K. Hazra, J.-K. Kim, J.-C. Jeon, H. Han, H. L. Meyerheim, T. Kontos, A. Cottet, and S. S. Parkin, *Nat. Nanotech.* **18**, 747 (2023).
- [66] F. S. Bergeret, A. F. Volkov, and K. B. Efetov, *Phys. Rev. Lett.* **86**, 4096 (2001).
- [67] A. F. Volkov, F. S. Bergeret, and K. B. Efetov, *Phys. Rev. Lett.* **90**, 117006 (2003).
- [68] F. S. Bergeret, A. F. Volkov, and K. B. Efetov, *Rev. Mod. Phys.* **77**, 1321 (2005).
- [69] A. I. Buzdin, *Rev. Mod. Phys.* **77**, 935 (2005).
- [70] J. Linder, T. Yokoyama, A. Sudbø, and M. Eschrig, *Phys. Rev. Lett.* **102**, 107008 (2009).
- [71] A. Cottet, *Phys. Rev. Lett.* **107**, 177001 (2011).
- [72] M. Eschrig, *Rep. Prog. Phys.* **78**, 104501 (2015).
- [73] E. A. Demler, G. B. Arnold, and M. R. Beasley, *Phys. Rev. B* **55**, 15174 (1997).
- [74] L. P. Gor’kov and E. I. Rashba, *Phys. Rev. Lett.* **87**, 037004 (2001).
- [75] P. A. Frigeri, D. F. Agterberg, A. Koga, and M. Sigrist, *Phys. Rev. Lett.* **92**, 097001 (2004).
- [76] F. S. Bergeret and I. V. Tokatly, *Phys. Rev. Lett.* **110**, 117003 (2013).
- [77] F. S. Bergeret and I. V. Tokatly, *Phys. Rev. B* **89**, 134517 (2014).
- [78] F. Crépin, P. Burset, and B. Trauzettel, *Phys. Rev. B* **92**, 100507 (2015).
- [79] M. Smidman, M. Salamon, H. Yuan, and D. Agterberg, *Rep. Prog. Phys.* **80**, 036501 (2017).
- [80] J. Cayao and A. M. Black-Schaffer, *Phys. Rev. B* **96**, 155426 (2017).
- [81] J. Cayao and A. M. Black-Schaffer, *Phys. Rev. B* **98**, 075425 (2018).
- [82] C. Fleckenstein, N. T. Ziani, and B. Trauzettel, *Phys. Rev. B* **97**, 134523 (2018).
- [83] I. V. Bobkova, P. J. Hirschfeld, and Y. S. Barash, *Phys. Rev. Lett.* **94**, 037005 (2005).
- [84] A. Kamra, A. Rezaei, and W. Belzig, *Phys. Rev. Lett.* **121**, 247702 (2018).
- [85] D. S. Rabinovich, I. V. Bobkova, and A. M. Bobkov, *Phys. Rev. Res.* **1**, 033095 (2019).
- [86] M. F. Jakobsen, K. B. Naess, P. Dutta, A. Brataas, and A. Qaiumzadeh, *Phys. Rev. B* **102**, 140504 (2020).
- [87] G. A. Bobkov, I. V. Bobkova, A. M. Bobkov, and A. Kamra, *Phys. Rev. B* **106**, 144512 (2022).
- [88] E. H. Fyhn, A. Brataas, A. Qaiumzadeh, and J. Linder, *Phys. Rev. Lett.* **131**, 076001 (2023).
- [89] P. Liu, J. Li, J. Han, X. Wan, and Q. Liu, *Phys. Rev. X* **12**, 021016 (2022).
- [90] H. Schiff, A. Corticelli, A. Guerreiro, J. Romhányi, and P. A. McClarty, *SciPost Physics* **18**, 109 (2025).
- [91] See Supplemental Material at [??] for the details of the construction of the $\mathbf{k} \cdot \mathbf{p}$ models, the derivation of pairing correlations and Josephson currents for Schrödinger and Dirac electrons, a comparison of the superconducting proximity effects for the two types of electrons, symmetry constraints on the spin texture and induced Cooper pairs, $0-\pi$ transitions in Josephson junctions, and supplementary numerical results for other choices of parameters. The Supplemental Material also contains Refs. [18, 97, 98, 107–110].
- [92] Y. Tanaka and A. A. Golubov, *Phys. Rev. Lett.* **98**, 037003 (2007).
- [93] J. Linder and A. V. Balatsky, *Rev. Mod. Phys.* **91**, 045005 (2019).
- [94] B. M. Andersen, I. V. Bobkova, P. J. Hirschfeld, and Y. S. Barash, *Phys. Rev. Lett.* **96**, 117005 (2006).
- [95] Y. Tanaka, Y. Tanuma, and A. A. Golubov, *Phys. Rev. B* **76**, 054522 (2007).

- [96] A. M. Black-Schaffer and A. V. Balatsky, *Phys. Rev. B* **88**, 104514 (2013).
- [97] M. P. L. Sancho, J. M. L. Sancho, and J. Rubio, *J. Phys. F: Met. Phys.* **14**, 1205 (1984).
- [98] M. P. L. Sancho, J. M. L. Sancho, J. M. L. Sancho, and J. Rubio, *J. Phys. F: Met. Phys.* **15**, 851 (1985).
- [99] D. Breunig, S.-B. Zhang, M. Stehno, and B. Trauzettel, *Phys. Rev. B* **99**, 174501 (2019).
- [100] S. H. Lee, Y. Qian, and B.-J. Yang, *Phys. Rev. Lett.* **132**, 196602 (2024).
- [101] L.-H. Hu and S.-B. Zhang, *Sci. China Phys. Mech. Astron.* **68**, 247211 (2025).
- [102] The ratio of between $\mathcal{F}_{\uparrow\uparrow}/\mathcal{F}_{\downarrow\downarrow}$ is approximately independent of position x .
- [103] H. Chen, T.-C. Wang, D. Xiao, G.-Y. Guo, Q. Niu, and A. H. MacDonald, *Phys. Rev. B* **101**, 104418 (2020).
- [104] Y. Zhang, Y. Sun, H. Yang, J. Železný, S. P. P. Parkin, C. Felser, and B. Yan, *Phys. Rev. B* **95**, 075128 (2017).
- [105] We neglect changes in the chemical potential μ when the materials are made into thin films.
- [106] I. Martin and C. D. Batista, *Phys. Rev. Lett.* **101**, 156402 (2008).
- [107] R. M. Fernandes, V. S. de Carvalho, T. Birol, and R. G. Pereira, *Phys. Rev. B* **109**, 024404 (2024).
- [108] J. Železný, Y. Zhang, C. Felser, and B. Yan, *Phys. Rev. Lett.* **119**, 187204 (2017).
- [109] Y. Zhang, J. Železný, Y. Sun, J. Van Den Brink, and B. Yan, *New J. Phys.* **20**, 073028 (2018).
- [110] S.-B. Zhang and B. Trauzettel, *Phys. Rev. Res.* **2**, 012018 (2020).